Nonlinear Slip Dynamics for an Omniwheel Mobile Robot Platform

Daniel Stonier, Se-Hyoung Cho, Sung-Lok Choi, Naveen Suresh Kuppuswamy, and Jong-Hwan Kim

Abstract— This study investigates the nonlinear dynamics of traction for an omniwheel mobile robot platform. A nonlinear slip model is incorporated into the dynamics of the system and the resulting equations of motion are derived using a Euler-Lagrange formulation. These are additionally transformed into slip-space, where the dynamical equations lend themselves to a convenient analysis of the slip dynamics. The conventional assumptions for ideal rolling are also explored and a reduced expression for the nonlinear dynamics is generated for such situations. Preliminary explorations toward a comprehensive analysis of the dynamics for omniwheel platforms under various control schemes is also initiated.

I. INTRODUCTION

Wheeled mobile robots are typically modelled as nonholonomic systems with an *ideal rolling* constraint. Whilst ideal rolling, the wheels of the mobile robot platform are assumed to roll without slipping. However, rolling conditions are often violated while the platform is accelerating or decelerating, resulting in a non-zero slip that can cause navigational error. In addition, certain slip states may deteriote and cause complete slippage (under acceleration) and lockup (under braking).

Previous works in mobile robot platforms for omniwheel motion systems often neglected the full import of these considerations [1], [2]. Subsequently, in this paper, the relevant dynamical theory is developed to explore the effects of slip and the performance of various control schemes for a mobile robot platform with an omniwheel motion system.

The dynamics presented here approximates the traction forces at work with a nonlinear slip model widely used in the field [3],[4]. The resulting equations of motion for the omniwheel platform are generated and also transformed to slip-space where it becomes convenient to investigate the stability of slip dynamics. The conventional dynamics for ideal rolling are also presented with a brief analysis of some of the typical assumptions made when implementing a control scheme for a system modelled on ideal rolling.

Section II introduces the architecture of the omnidirectional robot, utilizing the omniwheel platform, undergoing development in our laboratories. Section III develops the underlying dynamics fundamental to a comprehensive analysis of navigational motion for an omniwheel platform while Section IV provides a preliminary investigation into the more common control schemes used for mobile robot platforms.

II. OMNIDIRECTIONAL ROBOT PLATFORM

A. Motion Mechanism

One of important features for mobile robots is the ability to maneuver quickly and efficiently. To achieve this, many mobile robots adopt omnidirectional mechanisms that enable them to freely move without the constraints of a traditional mobile platform with the conventional differential drive.

Many different configurations exist for an omnidirectional platform. Some of these can provide omnidirectionality, but require the platform to reconfigure its internal state before major adjustments in its motion. One of the more popular arrangements however, ones utilizes mecanum wheels that allow freedom of motion without the necessity of reconfiguring its internal state. The omnidirectional robot currently under development in our laboratories possesses a three wheeled mecanum configuration. The mechanical design for the platform can be seen in Figure 1. It consists of three drive units comprising of a motor, a belt drive and omniwheel each. The design tries to maximize the utilization of space available underneath to accommodate the large motors.
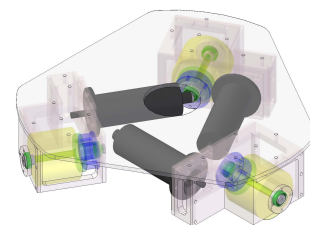

Fig. 1.   Mobile Robot Platform

Its design is configured for high performance, but it must also robustly handle a wide variety of surfaces and differing payloads in its environment. To obtain the accelerations required for high performance, 200W motors are used to drive the wheels. Subsequently, it is potentially possible for the robot to acquire an acceleration of $3m/s^2$ and a top speed of $3m/s$. Its ability to robustly handle a wide variety of environments however must be enabled through accurate dynamic modelling and robust control.

B. Vision System

The vision system employed on the mobile robot platform has the ability to use both dioptric and polydioptric vision systems .These provide a wide field of view that is assumed to be able to provide the mobile platform with accurate localisation data with a 360° field of view.

C. The System Architecture

The robot has been designed as shown in Figure 2. The architecture is modular and utilizes an onboard PC for the main processing unit.

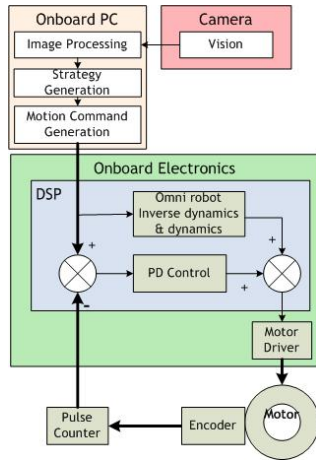The component subsystems of the onboard electronics and

Fig. 2.   The System Architecture

the software on the onboard PC can be seen in Figure 2. The onboard electronics consist of the control algorithm running on a TMS320C28xx series DSP module. The modular structure of the architecture enables efficient and parallel development of the component subsystems. The complete assembly
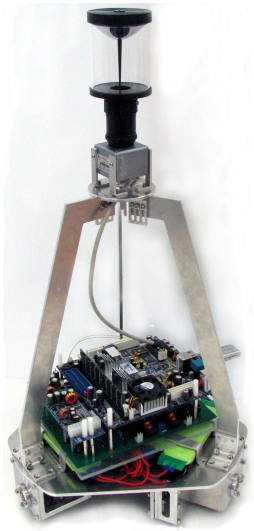

Fig. 3.   The complete robot assembly

of the robot with the catadioptric omnivision system fitted on can be seen in Figure 3.

III. Modelling

In this section we present three alternative methods for modelling the dynamics of an omniwheel mobile robot platform.

A. System Definition

The basic architecture of the wheeled platform is illustrated in Figure 4. A local frame of reference is fixed on the body of the robot at its centre of mass with basis vectors $\{e'_x, e'_y, e'_z\}$. The dynamics for this system can utilise these

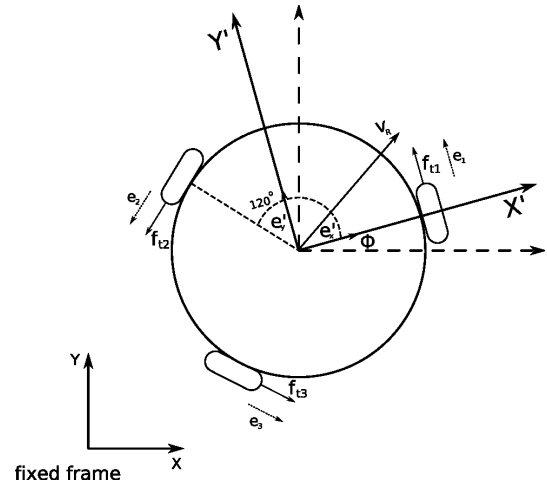Fig. 4.   Frames of Reference

rotating basis vectors or the basis fixed in the world frame $\{e_x, e_y, e_z\}$. If the robot is a differential drive robot, it is mathematically convenient to use the rotating set of basis vectors since the velocity and accelerations of the robot with respect to an observer on the robot are always in one direction (non-rotating). However, this advantage is nullified for an omnidirectional robot, so the following derivations will use the set of basis vectors fixed in the world frame for the dynamics calculations. Some transformations that will be used later are presented here for convenience.

$$
\begin{aligned}
e_1 &= e_y & e'_x &= \cos\phi\, e_x + \sin\phi\, e_y, \\
e_2 &= -(\sqrt{3}/2)\, e_x - (1/2)\, e_y & e'_y &= -\sin\phi\, e_x + \cos\phi\, e_y, \\
e_3 &= (\sqrt{3}/2)\, e_x - (1/2)\, e_y, & e'_z &= e_z
\end{aligned}
\tag{1}
$$

B. Traction Forces and Slip

Under ideal conditions, a rolling wheel moves without slipping. This constraint is such that a point on the wheel in contact with the ground is assumed to be instantaneously stationary with respect to the ground. When this condition is not met, the wheel is said to be undergoing slip. This can be in the form of genuine slipping (under acceleration) or skidding (under braking). The mathematical definition of slip for a single wheel is given by

$$
s = \frac{(r_w\omega - v)}{\max\{r_w\omega, v\}},
\tag{2}
$$

where ω, v are the angular and linear velocity of a wheel with radius r_ω. The equation is normalised so that the slip variable is constrained to $-1 \leq s \leq 1$. The wheel is said to be *ideal rolling* if it maintains a state of no-slip ($s = 0$, $\dot{s} = 0$).

When no torque is applied to the wheel, it can be verified that ideal rolling is an asymptotically stable mode, where

the only friction at work is a minimal *rolling friction*. However, under the presence of a non-zero torque, this mode becomes asymptotically unstable and the wheel will commence slipping (or skidding if braking). When the wheel is slipping, a corresponding frictional force is generated. This force is referred to as the *traction force* and it is significantly larger than the rolling friction. Experimental results indicate traction forces are of the form $f_t = \mu_a(s)N$ where N is the normal force and the *adhesive co-efficient function*, $\mu_a(s)$ closely matches a nonlinear function that is dependant on the surface type. Figure 5 illustrates measured estimates for the adhesive co-efficient on a variety of surfaces ranging from dry asphalt (a) through to packed snow (d). Most surfaces fall inbetween (a) and (b).
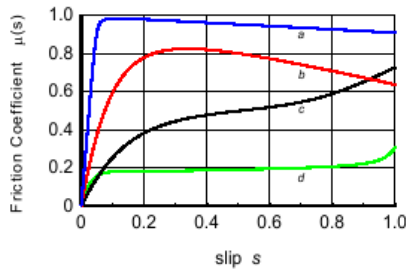

Fig. 5.   Empirical Estimates of the Adhesive Co-efficient

In these measurements, the negligible effects of rolling friction (in comparison to the tractive forces) have been ignored. An efficient formula for numerical algorithms that captures the salient features of the adhesive co-efficients is given by

$$\mu_a(s) = c_1(1 - e^{-c_2 s}) - c_3 s. \qquad (3)$$

It can also be shown via a theoretical analysis [4], that under suitably low torques, wheel slips will converge to a non-zero, steady-state slip mode. This observation indicates that there will always be slip error under acceleration or braking.

Under higher torques, this steady state slip mode bifurcates and eventually collapses again, leading to *100% slippage* under acceleration, or *lockup* under braking.

To cater for the effects of slip, some simulation and experimentation is needed to determine the extent of the errors caused by the steady state slip modes as well as the critical torques that precede bifurcation and complete instability.

C. Euler-Lagrange Dynamics

We utilise the standard Euler-Lagrangian formulation for the dynamics of the system.

$$\frac{d}{dt}\left[\frac{\partial \mathcal{L}}{\partial \dot{q}_i}\right] - \frac{\partial \mathcal{L}}{\partial q_i} = \mathcal{F}_i \qquad (4)$$

where the q_i are the generalised co-ordinates of the system listed previously and the $\mathcal{F}_i$ are the corresponding generalised forces not derivable from a potential field.

1) Generalised Co-ordinates: The mobile robot platform is a 6DOF system. Three variables are needed for world configuration (position and orientation with respect to a world frame) and three for internal configuration (wheel orientations). These are denoted by $\boldsymbol{q} = [x, y, \phi]^T$ and $\boldsymbol{\theta} = [\theta_1, \theta_2, \theta_3]^T$ respectively.

2) Generalised Forces: The external forces are derived from the torque τ_i at the motors and the traction forces f_{t_i} at each wheel contact. The generalised forces corresponding to the generalised co-ordinates defined previously are of the form

$$\begin{aligned} \mathcal{F}_q &= Q(\phi)\boldsymbol{f}_t, \\ \mathcal{F}_\theta &= \boldsymbol{\tau} - r_w \boldsymbol{f}_t \end{aligned} \qquad (5)$$

where

$$Q(\phi) = \begin{bmatrix} -\sin(\phi) & -\sin(\phi+2\pi/3) & -\sin(\phi+4\pi/3) \\ \cos(\phi) & \cos(\phi+2\pi/3) & \cos(\phi+4\pi/3) \\ r & r & r \end{bmatrix}$$

Here r is the radius of the mobile robot platform and r_w is the wheel radius.

3) Lagrangian: The Lagrangian is simply a function of the Kinetic Energy of the mobile robot platform.

$$\mathcal{L} = \frac{1}{2}\left\{ m(\dot{x}^2 + \dot{y}^2) + I_R \dot{\phi}^2 + \sum_{i=1}^{3} I_w \dot{\theta}_i^2 \right\} \qquad (6)$$

where I_R is the moment of inertia of the robot and I_w is the moment of inertia of each wheel.

D. Nonlinear E-L Dynamics

Substituting (5),(6) into (4) we obtain in matrix form,

$$\begin{aligned} M\ddot{\boldsymbol{q}} &= Q(\phi)\boldsymbol{f}_t, & (7) \\ I_w \ddot{\boldsymbol{\theta}} &= \boldsymbol{\tau} - r_w \boldsymbol{f}_t. & (8) \end{aligned}$$

where

$$M = \begin{bmatrix} m & 0 & 0 \\ 0 & m & 0 \\ 0 & 0 & I_R \end{bmatrix}.$$

and m, I_R are the mass and moment of inertia of the mobile robot platform, while r_w, I_w are the radius and moment of inertia of each wheel. This represents the full (slip included) nonlinear dynamics for the mobile robot platform. Each traction force is of the form $f_{t_i} = \mu_a(s_i)N$ and thus depends nonlinearly on the slip. The representation used for the adhesive co-effecient is given by (3).

E. Nonlinear E-L Dynamics $((\boldsymbol{q}, \boldsymbol{s})$ space)

The nonlinear functions (7) and (8) utilise the state variables $\boldsymbol{q}, \boldsymbol{\theta}$. However, since slip is a function of both robot and wheel states (2), it is possible to investigate the nonlinear dynamics using the pair of independant state variables $(\boldsymbol{q}, \boldsymbol{s})$ rather than the usual pairing of $(\boldsymbol{q}, \boldsymbol{\theta})$. This provides an elegant and meaningful interpretation of the dynamics.

1) Wheel Velocity: For an omnidirectional robot, the slip (2) for the i-th wheel under braking is defined as

$$s_i = \frac{(r_w \dot\theta_i - v_{w_i})}{v_{w_i}},$$

where v_{w_i} is the velocity of the i-th wheel with respect to the world frame. The individual wheel velocities are given by

$$v_{w_i} = \boldsymbol{v} \cdot \boldsymbol{e}_i + r\dot\phi,$$
$$= (\dot x \boldsymbol{e}_x + \dot y \boldsymbol{e}_y) \cdot \boldsymbol{e}_i + r\dot\phi,$$

where $\boldsymbol{v} = (\dot x \boldsymbol{e}_x + \dot y \boldsymbol{e}_y)$ is the velocity of the centre of mass of the robot and the $\boldsymbol{e}_i$ are the unit vectors aligned in the direction of each wheel (refer to Figure 4). Substituting the expressions from (1) for each wheel,

$$v_{w_1} = -v_x \sin\phi + v_y \cos\phi + r\dot\phi,$$
$$v_{w_2} = -v_x\left(-\tfrac{\sqrt 3}{2}\cos\phi + \tfrac12\sin\phi\right) + v_y\left(-\tfrac{\sqrt 3}{2}\sin\phi - \tfrac12\cos\phi\right) + r\dot\phi,$$
$$v_{w_3} = -v_x\left(\tfrac{\sqrt 3}{2}\cos\phi + \tfrac12\sin\phi\right) + v_y\left(\tfrac{\sqrt 3}{2}\sin\phi - \tfrac12\cos\phi\right) + r\dot\phi.$$

In matrix form,

$$\boldsymbol{v}_w = RT(\phi)\dot{\boldsymbol{q}}, \tag{9}$$

where

$$R = \begin{bmatrix} 0 & 1 & r \\ -\sqrt 3/2 & -1/2 & r \\ \sqrt 3/2 & -1/2 & r \end{bmatrix} \quad T(\phi) = \begin{bmatrix} \cos\phi & \sin\phi & 0 \\ -\sin\phi & \cos\phi & 0 \\ 0 & 0 & 1 \end{bmatrix}$$

Subsequently,

$$\dot{\boldsymbol{v}}_w = RT(\phi)\ddot{\boldsymbol{q}} + \dot\phi RT'(\phi)\dot{\boldsymbol{q}},$$
$$= RT(\phi)M^{-1}Q(\phi)\boldsymbol{f}_t + \dot\phi RT'(\phi)\dot{\boldsymbol{q}}, \tag{10}$$

where we have substitued for the acceleration $\ddot{\boldsymbol{q}}$ from (7).

2) The Slip Equation: Returning to the dynamics, the second of the E-L equations (8) can be transformed to the slip space s in the following manner. First we derive the rate of change of slip for the i-th wheel.

$$\dot s_i = \frac{(r_w\ddot\theta_i - \dot v_{w_i})}{v_{w_i}} - \frac{(r_w\dot\theta_i - v_{w_i})\dot v_{w_i}}{v_{w_i}^2},$$
$$= \frac{(r_w\ddot\theta_i v_{w_i} - r_w\dot\theta_i \dot v_{w_i})}{v_{w_i}^2},$$
$$v_{w_i}^2 \dot s_i = r_w\left(\frac{\tau_i - r_w f_{t_i}}{I_w}\right)v_{w_i} - v_{w_i}(s_i+1)\dot v_{w_i},$$
$$v_{w_i}\dot s_i = \left[\left(\frac{r_w}{I_w}\right)\tau_i - \left(\frac{r_w^2}{I_w}\right)f_{t_i} - (s_i+1)\dot v_{w_i}\right],$$

In matrix form,

$$V_w\dot{\boldsymbol{s}} = \frac{r_w}{I_w}\left[\boldsymbol{\tau} - M^*(s)M^{-1}Q(\phi)\boldsymbol{f}_t - N^*\dot{\boldsymbol{q}}\right],$$

where

$$S = \text{diag}(\boldsymbol{s}),$$
$$V_w = \text{diag}(\boldsymbol{v}_w),$$
$$N^* = \dot\phi\frac{I_w}{r_w}(S+I)RT'(\phi),$$
$$M^*(\boldsymbol{s}) = rQ^{-1}(\phi)M + \frac{I_w}{r_w}(S+I)RT(\phi).$$

Subsequently the full nonlinear E-L dynamics in the $(\boldsymbol{q}, \boldsymbol{s})$ space under braking is given by

$$M\ddot{\boldsymbol{q}} = Q(\phi)\boldsymbol{f}_t,$$
$$V_w\dot{\boldsymbol{s}} = \frac{r_w}{I_w}\left[\boldsymbol{\tau} - M^*(s)M^{-1}Q(\phi)\boldsymbol{f}_t - N^*\dot{\boldsymbol{q}}\right]. \tag{11}$$

Similar equations may be generated for accelerational slip dynamics.

F. Ideal Rolling E-L Dynamics

Ideal rolling introduces three constraints to the dynamics. Each constraint is of the form $s_i = \dot s_i = 0$. Substituting these constraints directly into (11) and eliminating $\boldsymbol{f}_t$, the constrained dynamics for ideal rolling can be represented by

$$M^*\ddot{\boldsymbol{q}} + N^*\dot{\boldsymbol{q}} = \boldsymbol{\tau}, \tag{12}$$

where

$$M^* = M^*(\boldsymbol{0}).$$

Under ideal rolling, the traction forces are assumed to be able to generate the required torques to sustain ideal rolling (ensuring the contact point remains stationary) in a similar fashion to the manner in which static friction ensures a block will remain stationary on a flat surface. The exact relationship between torque and traction force can be determined directly from (11) by setting $\boldsymbol{s} = \dot{\boldsymbol{s}} = 0$,

$$\boldsymbol{\tau} = M^*M^{-1}Q(\phi)\boldsymbol{f}_t + N^*\dot{\boldsymbol{q}}. \tag{13}$$

IV. CONTROL

The dynamics models generated in the previous section now allow us to undertake a comprehensive analysis of various control schemes. These will be performed both in simulation and in experiments and used to evaluate the performance of each scheme as well. In some cases, the effects of unmodelled slip dynamics will also be explored. In this paper we present a few preliminary results to highlight the use of the dynamics.

A. Computed Torque Control

Computed torque control utilises a feedback linearising transformation of the form

$$\boldsymbol{\tau} = M^*(\ddot{\boldsymbol{q}}_d - \boldsymbol{u}) + N^*\dot{\boldsymbol{q}}. \tag{14}$$

where $\boldsymbol{u}$ is the control input, or outer loop control, while $\boldsymbol{\tau}$ is referred to as the inner loop control. If we assume an ideal rolling dynamics model, substituting this into (12) yields the error dynamics:

$$\ddot{\boldsymbol{e}} = \boldsymbol{u}.$$

The primary advantage of this method is that the feedback linearisation allows complete customisation of the error dynamics. Its main drawback however, is that it is not a decoupled control strategy. The inclusion of M^* and N^* in the torque (14) require that the orientation of the robot be known in order to compute the required torque for any single wheel.

1) PD Computed Torque Controller: There are various ways that the outer loop control, $\boldsymbol{u}$ may be defined. Here, we simply set

$$\boldsymbol{u} = -K_v \dot{\boldsymbol{e}} - K_p \boldsymbol{e}. \qquad (15)$$

where $\boldsymbol{e} = \boldsymbol{q}_d - \boldsymbol{q}$. The closed loop error dynamics are

$$\ddot{\boldsymbol{e}} + K_v \dot{\boldsymbol{e}} + K_p \boldsymbol{e} = 0. \qquad (16)$$

K_v and K_p are simply chosen to ensure a desired error convergence rate. In the case of unmodelled disturbances, PD control returns a non-zero steady state error. In this case, a PID controller may be substituted to improve the error convergence.

2) Computed Torque Like Controller: The computed torque technique can provide some level of robustness given either small disturbances or uncertain knowledge regarding the exact representation for M^* and N^*. In this case the following modified control law may be used.

$$\boldsymbol{\tau} = \hat{M}^*(\ddot{\boldsymbol{q}}_d - \boldsymbol{u}) + \hat{N}^* \dot{\boldsymbol{q}}.$$

A Lyapunov proof using Lasalle's Theorem and Barbalat's Lemma provide some assurance of ensuring a desired error convergence for a PD or PID scheme so long as the outer loop gains are chosen large enough.

B. Workspace Control

Workspace control is performed in the global configuration space (x, y, ϕ). Errors are used to generate the required generalised forces for convergent error dynamics.

$$Q(\phi)\boldsymbol{f}_t = K_d \dot{\boldsymbol{e}} + K_p \boldsymbol{e},$$

Substituting this into (7), the closed loop error dynamics are given by

$$\ddot{\boldsymbol{e}} + K_v \dot{\boldsymbol{e}} + K_p \boldsymbol{e} = \ddot{\boldsymbol{q}}_d + (I - M^{-1})(K_v \dot{\boldsymbol{e}} + K_p \boldsymbol{e}), \quad (17)$$

where the right hand side is treated as a disturbance and K_v, K_p are tuned appropriately. The actual torque required from the motors is derived from (13),

$$\boldsymbol{\tau} = M^* M^{-1} Q(\phi) \boldsymbol{f}_t + N^* \dot{\boldsymbol{q}},$$
$$= (r_w + \frac{I_w}{r_w} RT(\phi) M^{-1} Q) Q^{-1}(K_d \dot{\boldsymbol{e}} + K_p \boldsymbol{e}) + N^* \dot{\boldsymbol{q}}.$$

where $\boldsymbol{f}_t = Q^{-1}(K_d \dot{\boldsymbol{e}} + K_p \boldsymbol{e})$. In practice, M may not be accurately known and the torque is often more simply modelled by the approximation given by $\boldsymbol{\tau} \approx r_w \boldsymbol{f}_t$. This is often justifiable as typically the model parameters ensure $r_w >> \frac{I_w}{r_w} RT(\phi) M^{-1} Q$ and N^* is small (low spin). For our robot, $r_w \approx 25(I_w/r_w) RT(\phi) M^{-1} Q$.

C. Classic Kinematic Control

A classic kinematic controller uses an inner/outer loop strategy that defines a suitable reference workspace velocity that is passed through the inverse kinematics before sending it to the motor controller. Outer loop calculations (reference velocity and IK transformation) are given as follows:

$$\dot{\boldsymbol{q}}_r = \dot{\boldsymbol{q}}_d + K_v \dot{\boldsymbol{e}} + K_p \boldsymbol{e}.$$
$$\dot{\boldsymbol{\theta}}_r = (1/r_w) RT(\phi) \dot{\boldsymbol{q}}_r.$$

In the inner loop, for best results, a dynamic controller can be used to ensure tracking of the referential angular velocity, however this still requires knowledge of the inertial parameters of the robot and motor subsystem. The simpler strategy is to use a simple PD controller of the form

$$\boldsymbol{\tau} = K_{v_\theta} \dot{\boldsymbol{e}}_\theta, \qquad (18)$$

where $\dot{\boldsymbol{e}}_\theta = \dot{\boldsymbol{\theta}}_r - \dot{\boldsymbol{\theta}}$.

D. Simulation

Ideal rolling dynamics (12) were used for this simulation in which the various controllers were tested on different input trajectories. The purpose of the simulations are to investigate the error convergence of each controller under varying accelerational conditions (this is also analogous to systems having to cope with varying payloads). This is particularly important for platforms which require responsive behaviour in conditions which require frequent and varying accelerations/decellerations (robot soccer or environments that generate curved motions).

In each of the simulations, the robot was instructed to move in a straight line (y-direction) under varying accelerations

- Zero acceleration
- Constant acceleration
- Linearly varying acceleration
- Constant spin + Constant acceleration

These trajectories were tested with each of the four controllers mentioned previously.

- Computed Torque (CT)
- Workspace Control with Model Parameters (WC1)
- Workspace Control without Model Parameters (WC2)
- Classic Kinematic Controller (K)

1) Zero Acceleration: Under constant velocity ($\ddot{\boldsymbol{q}}_d = 0$), gain parameters for the workspace and classic kinematic controller may be tuned to match the error convergence dynamics of the computed torque controller (note that the gains will be different in each case - consider, for example, re-arranging (17) for error dynamics that would match (16)). This is illustrated in Figure 6 where gains for each controller were chosen to match error dynamics with $K_v = 10, K_p = 15$.

2) Constant Acceleration: Under the presence of an acceleration, only the computed torque controller remains free from a non-zero disturbance in dynamics. This affects the error convergence dynamics (either slowing convergence or causing excessive overshoot depending on the sign of the
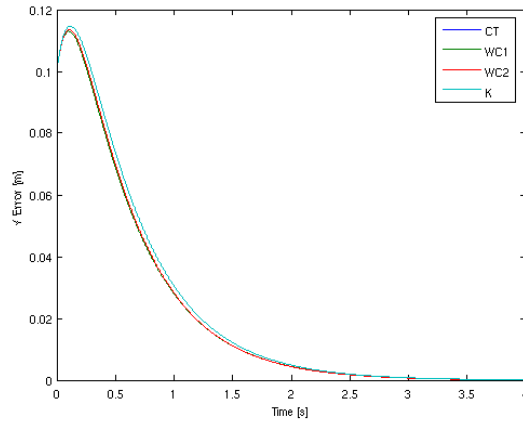
2371

Fig. 6.   Error Dynamics under Zero Acceleration

Fig. 8.   Error Dynamics under Ramped Acceleration

acceleration) and also introduces a non-zero steady state error. This could be suppressed with the appropriate gains, but then this would in turn affect the nature of the error convergence dynamics under constant velocity. The effects of this can be seen in Figure 7 where the dynamic controller (CT) has zero steady state error and the remaining controllers have progressively larger steady state errors (WC1, WC2, K respectively).
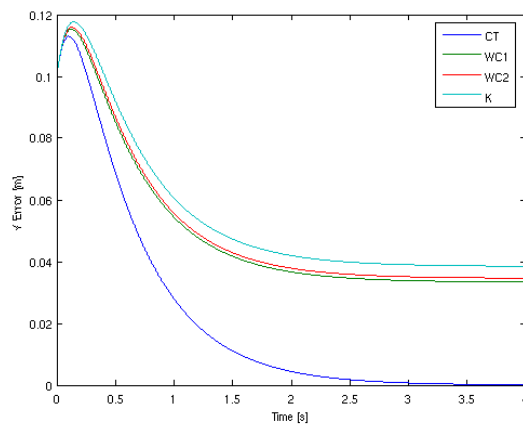

Fig. 7.   Error Dynamics under High Acceleration

3) Varying Acceleration: Here the acceleration was increased linearly from 0 to 1 (ramp function). This is illustrated in Figure 8 where it can be seen that the steady state errors increase as a function of the acceleration.

4) Non-Zero Spin Velocity: In the previous examples, WC1 and WC2 match each other quite closely and WC2 appears to be a good approximation for WC1. The most significant difference occurs when $\dot{\phi} \neq 0$ as this directly affects the magnitude of N^*. However, variation between the error dynamics between WC1 and WC2 remains negligible ($< 1\%$).

5) Summary: If responsive behaviour for varying accelerations is required, a dynamic controller (CT) can ensure consistent error convergence dynamics. The remainder can
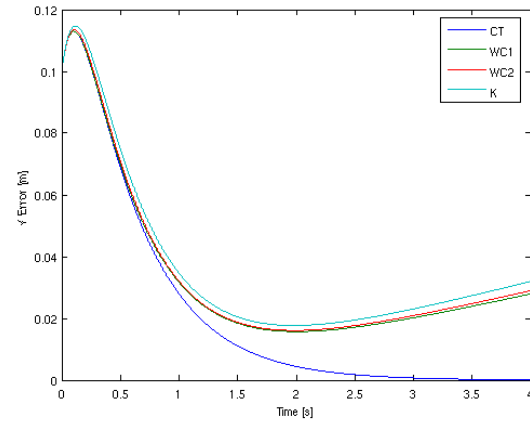
be tuned, but error convergence dynamics will either lag (as illustrated here) or overshoot as accelerational or inertial conditions vary. They also exhibit an unavoidable steady state error. These are progressively more pronounced as more and more of the dynamics is removed from the calculations. These effects also translate to variations in torque magnitudes under different accerational conditions when there is an error.

V. Conclusion

In this paper we have presented the fundamental nonlinear slip dynamics for an omniwheel mobile robot platform and initiated a preliminary investigation of controllers for navigation of such a system. Our future work will investigate the development of a controller that utilizes an understanding of the steady state slip modes to improve performance when compared with that obtained under an ideal rolling assumption. This will enable investigation of the effect of the nonlinear slip dynamics with the conventional controllers and the usage of sliding or adaptive controllers to improve performance on a wide variety of surfaces and varying payloads. The nonlinear dynamics transformed into the (q, s) space should also provide a useful tool for exploring the emergence, bifurcation and collapse of steady state slip modes for an omniwheel mobile robot platform.

References

[1] R. Rojas and A. Forster, "Holonomic control of a robot with an omnidirectional drive," *Kunstliche Intelligenz*, 2006.
[2] R. Williams, B. Carter, P. Gallina, and G. Rosati, "Dynamic model with slip for wheeled omnidirectional robots," *IEEE Transactions on Robotics and Automation*, vol. 18, no. 3, 2002.
[3] C. Wit, P. Tsiotras, and E. Velenis, "Dynamic friction models for longitudinal road/tire interaction: Theoretical advances," *Proceedings of Modelling, Identification, and Control*, 2002.
[4] B. Olson, S. Shaw, and G. Stepan, "Nonlinear dynamics of vehicle traction," *Vehicle System Dynamics*, vol. 40, no. 6, pp. 377–399, 2003.
[5] C. Geyer, "Short course on omnidirectional vision," *International Conference on Computer Vision*, October 2003.
[6] Y. Li, D. Oetomo, and H. Macelo, "Torque distribution and slip minimization in an omnidirectional mobile base," *Proceedings of International Conference on Advanced Robotics*, pp. 567–572.
[7] T. Nagy, R. D'Andrea, and P. Ganguly, "Near-optimal dynamic trajectory generation and control of an omnidirectional vehicle," *Robotics and Autonomous Systems*, vol. 46.